◆ Human Brain Mapping 36:3117–3136 (2015) ◆

Towards a Functional Atlas of Human White Matter

Silvio Sarubbo,[1,2] Alessandro De Benedictis,[3] Stefano Merler,[4] Emmanuel Mandonnet,[5] Sergio Balbi,[6] Enrico Granieri,[2] and Hugues Duffau[7,8]*

[1]*Department of Neurosciences, Division of Neurosurgery, "S. Chiara" Hospital, Trento, Italy*
[2]*Department of Biomedical and Surgical Sciences, Section of Neurological, Psychiatric and Psychological Sciences, "S. Anna" University–Hospital, Ferrara, Italy*
[3]*Department of Neuroscience and Neurorehabilitation, Neurosurgery Unit, Bambino Gesù Children's Hospital–IRCCS, Roma, Italy*
[4]*Bruno Kessler Foundation, Trento, Italy*
[5]*Department of Neurosurgery, Lariboisiere Hospital, Paris, France*
[6]*Department of Biotechnologies and Life Sciences, Ph.D. School in Surgery and Surgical Biotechnologies, University of Insubria, Varese, Italy*
[7]*Department of Neurosurgery, Gui de Chauliac Hospital, Montpellier University Medical Center, Montpellier, France*
[8]*Team "Plasticity of Central Nervous System, Stem Cells and Glial Tumors," INSERM U1051, Institute for Neuroscience of Montpellier, Saint Eloi Hospital, Montpellier, France*

Abstract: *Objectives:* Although diffusion tensor imaging (DTI) and *postmortem* dissections improved the knowledge of white matter (WM) anatomy, functional information is lacking. Our aims are: to provide a subcortical atlas of human brain functions; to elucidate the functional roles of different bundles; to provide a probabilistic resection map of WM. *Experimental design:* We studied 130 patients who underwent awake surgery for gliomas (82 left; 48 right) with electrostimulation mapping at cortical and subcortical levels. Different aspects of language, sensori-motor, spatial cognition, and visual functions were monitored. 339 regions of interest (ROIs) including the functional response errors collected during stimulation were co-registered in the MNI space, as well as the resections' areas and residual tumors. Functional response errors and resection areas were matched with DTI and cortical atlases. Subcortical maps for each function and a probability map of resection were computed. *Principal observations:* The medial part of dorsal stream (arcuate fasciculus) subserves phonological processing; its lateral part [indirect anterior portion of the superior longitudinal fascicle (SLF)] subserves speech planning. The ventral stream subserves language semantics and matches with the inferior fronto-occipital fascicle. Reading deficits match with the inferior longitudinal fascicle. Anomias match with the indirect posterior portion of the SLF. Frontal WM underpins motor planning and execution. Right parietal WM subserves spatial cognition. Sensori-motor and visual fibers were the most preserved bundles. *Conclusions:* We report the first anatomo-functional atlas of WM connectivity in humans by correlating cogni-

Additional Supporting Information may be found in the online version of this article.

***Correspondence to**: Hugues Duffau, M.D., Ph.D., Department of Neurosurgery, Gui de Chauliac Hospital, Montpellier University Medical Center, 80 Avenue Augustin Fliche, 34295 Montpellier, France. E-mail: h-duffau@chu-montpellier.fr

Received for publication 7 October 2014; Revised 18 April 2015; Accepted 20 April 2015.

DOI: 10.1002/hbm.22832
Published online 9 May 2015 in Wiley Online Library (wileyonlinelibrary.com).

tive data, electrostimulation, and DTI. We provide a valuable tool for cognitive neurosciences and clinical applications. *Hum Brain Mapp 36:3117–3136, 2015*.

Key words: subcortical atlas; direct electrical stimulation; white matter pathways; functional connectivity

INTRODUCTION

Over the last century, the modern neuroscientific research significantly advanced toward a more realistic comprehension of the anatomo-functional basis underlying brain processing. As opposed to the traditional localizationist concept of a rigid "one region–one function" correlation, growing evidences have been provided in favor of a more dynamic vision of the central nervous system (CNS) as a complex network [Borner et al. 2007, Bressler and Tognoli, 2006, McIntosh et al. 2000, Reijneveld et al. 2007], opening the era of the brain "connectome." It consists of a mosaic of cortical neuronal hubs, interconnected at short and long range by widely integrated, parallel and often redundant axonal subcircuits [Sporns et al, 2005; Sporns, 2013a, 2013b]. According to this insight, a neurological function results from the multimodal interaction between multiple crucial functional epicentres regulated by modulator areas.

This conceptual advance has been supported by a methodological evolution of structural and functional techniques, such as resting state functional magnetic resonance imaging (RS-fMRI), magnetoencephalography (MEG), and diffusion tensor imaging (DTI), allowing to investigate noninvasively and "in vivo" several complex properties of brain networks. Particularly, RS-fMRI and MEG are clarifying the organization of the functional areas, the plastic potential of brain networks and the balancing among different neural circuits by means of even more appropriate and specific neurophysiological and neuropsychological tasks. On the other hand, as demonstrated by recent structural and functional studies, the influence, segregation, and

Abbreviations

AF	arcuate fascicle
AG	angular gyrus
Calc	calcarine cortex
Caud	caudate
CC	corpus callosum
Cing	cingulum
CNS	central nervous system
CST	cortico-spinal tract
CTT	cortico-thalamic tract
DES	direct electrical stimulation
DLPFC	dorso-laterale pre-frontal cortex
DO-80	denomination object 80
DTI	diffusion tensor Imaging
EC	external capsule
fMRI	functional MRI
IC	internal capsule
IFG	inferior frontal gyrus
IFOF	inferior fronto-occipital fascicle
ILF	inferior longitudinal fascicle
IOG	inferior occipital gyrus
IPL	inferior parietal lobule
ITG	inferior temporal gyrus
LGG	low-grade glioma
MdLF	middle longitudinal fascicle
MedFOG	medial fronto-orbital gyrus
MEG	magnetoencephalography
MFG	middle frontal gyrus
MidFOG	middle fronto-orbital gyrus
MNI	Montreal Neurological Institute
MOG	middle occipital gyrus
MTG	middle temporal gyrus
MTP	middle temporal pole
NRP	nonresection probability
OpIFG	pars opercularis of inferior frontal gyrus
OR	optic radiation
OrbIFG	pars orbitalis of inferior frontal gyrus
OrbMFG	orbital middle frontal gyrus
OrbSFG	orbital superior frontal gyrus
ParaCL	parac-central lobule
PreCG	pre-central gyrus
RolOP	rolandic opercula
PostCG	post-central gyrus
PostCL	post-central lobule
preSMA	pre-supplementary motor area
Put	putamen
RS-fMRI	resting state-functional MRI
ROI	region of interest
RVP	residual volume probability
SCF	subcallosal fascicle
SFG	superior frontal gyrus
SFOG	superior fronto-orbital gyrus
SLF	superior longitudinal fascicle
SMA	supplementary motor area
SMG	supra-marginal gyrus
SOG	superior occipital gyrus
SPL	superior parietal lobule
STG	superior temporal gyrus
STP	superior temporal pole
TrIFG	pars triangularis of inferior frontal gyrus
UF	uncinate fascicle
VPMC	ventral pre-motor cortex
WHO	World Health Organization
WM	white matter

integration of the different networks are strongly related to their connectivity patterns, including density, length, number and distribution of fibers, which connect the functional-related structures (i.e. nodes, modules, hubs, rich clubs) [Collin et al. in press, Sporns, 2013a, 2013b].

In this context, WM is of primary relevance, since it represents the structural substrate for brain connectivity [Filley, 2005]. Recently, DTI strongly renewed the interest for the knowledge of WM anatomical features [Catani and Ffytche, 2005], providing even more reliable reconstructions of the course of the main bundles and relationships among them [Thiebaut de Schotten et al., 2011]. Currently, the crucial role of connectivity for functional processing is supported also by the results provided by the direct electrical stimulation (DES) technique, adopted during resections of brain tumors, in order to recognize and preserve the eloquent structures [Duffau, 2008]. Particularly, low-grade gliomas (LGGs) are slow growing (4–5 mm/year) but not benign tumors [Mandonnet et al, 2007]. The main features of these lesions are, in fact, the inescapable anaplastic transformation (after 7–8 years) and the frequent invasion of eloquent cortices and subcortical pathways [Duffau, 2005]. The use of intraoperative DES for mapping the subcortical region in awake patients opened a new door in the treatment of these lesions and constitutes an unprecedented opportunity to assess the functional role of different pathways [Duffau, 2008; Duffau et al., 2013]. Moreover, increasing experiences are also demonstrating that extensive resections, even if involving high-eloquent cortical regions, may not produce postoperative permanent deficits if the eloquent connectivity identified by DES is preserved [Duffau, 2008].

Nevertheless, although these results have contributed to increase our knowledge considerably, the crucial role of WM in the organization of brain networks still needs to be further clarified, from both anatomical (i.e. the course, segmentation and terminations of the WM tracts) and functional perspectives.

The first aim of the present study is to advance in the knowledge of the WM functional anatomy, providing a functional subcortical atlas for experimental and clinical purposes, structured on DES data obtained from a large and homogenous population–particularly focusing on the phonologic, semantic and syntactic aspects of language elaboration, as well as the visual, motor and sensory functions. Second, we aim to elucidate a possible functional role of specific bundles, including the inferior fronto-occipital fascicle (IFOF), the arcuate fascicle (AF), the indirect posterior and anterior portions of the superior longitudinal fascicle (SLF), the inferior longitudinal fascicle (ILF), the optic radiation (OR), the subcallosal fascicle (SCF), the cortico-spinal tract (CST) and somato-sensorial (SS) fibers of the cortico-thalamic tract (CTT), the corpus callosum (CC), and the cingulum (Cing). To this end, we analyzed the spatial relationships between collected functional response errors from DES and the structural data, as described in the DTI Atlas by Thiebaut de Schotten et al. (2011). Finally, we discussed the structural implications, arising from the integrated anatomo-functional analysis of the course, terminations and segmentations of these tracts.

MATERIALS AND METHODS

Patients and Surgical Methods

We selected 130 cases [72 males and 58 females; mean age: 38.9 years; SD: 9.9] with WHO grade II LGGs infiltrating eloquent cortical and subcortical areas. 82 lesions involved the left and 48 the right hemisphere. No patients experienced pre-operative neurological deficits and 88% were symptomatic for seizures. 111 patients were right-handers, 12 were left-handers, and 7 were ambidextrous. They underwent surgery according to asleep-awake-asleep protocol, with total intravenous anaesthesia using Remifentanil and Propofol infusion stopped before the awake surgical step. Park bench position was adopted in all cases. Cortico-subcortical DES was performed to obtain the most sensitive and specific identification of the main subcortical pathways, according to the technique previously reported by the senior author (H.D.) [Duffau et al., 2005, 2008] and first described by Ojemann and Berger [Berger et al., 1990; Ojemann et al., 1989]. A bipolar electrode with 5 mm spaced tips delivering a biphasic current (pulse frequency of 60 Hz; single-pulse phase duration of 1 ms; amplitude between 1 and 4 mA) was used in all cases. During the awake step, the intensity threshold was set either by evoking a pure speech arrest (without facial or tongue movements) at the DES of the VPMC or by evoking motor (i.e. muscle contraction) or sensory (i.e. dysesthesias) responses at the stimulation of the primary motor or sensory area, within the precentral or postcentral gyrus (PreCG and PostCG, respectively). The minimum intensity used in this series was 2 mA and the maximum 4 mA (mean 2.8 mA). The complete cortical mapping was achieved according to other selected functional tasks and then, the resection started. During this phase, the patients were asked to perform continuously specific tasks, according to the eloquent role of the bundles that the neurosurgeon expects to encounter over the different steps of resection. Again, subcortical mapping of the white matter pathways was performed using DES with the same electrical parameters as at the cortical level. When all functional limits were reached (i.e. the boundaries of the surgical cavities resulted in eloquent responses at DES, identified by numeric tags, both at the cortical and the subcortical level), the resection was stopped and the patient was asleep again. Following completion of resection, intraoperative pictures were taken and subsequently analyzed offline.

Intraoperative Functional Monitoring

Intraoperative neuropsychological monitoring was assessed according to the lesion's site, and to the expected eloquent cortico-subcortical structures encountered during the resection [Fernàndez Coello et al., 2013]. According to

the technique, we previously described [Duffau et al., 2005, 2008], motor functions were monitored with a continuous complex task (hand, arm and forearm flexion-extension contralateral to the lesion side) and the sensory responses were directly reported from the patients during cortical and subcortical mapping and collected by the neuropsychologist throughout the surgery. The spontaneous language production was monitored with counting test (series from 0 to 10) and repetition test [Fernàndez Coello et al., 2013]. The phonologic and semantic aspects of language processing (i.e. semantic and phonological paraphasias; pure anomia, not related to motor, praxic and visual disturbances nor associate to semantic or phonological deficits) and reading (i.e. alexia or reading disturbances) were assessed, respectively, with the naming [denomination object 80 (DO 80)] and reading test, as previously reported [Duffau et al., 2003a, 2003b; Duffau et al., 2005; Duffau, 2008; Fernàndez Coello et al., 2013; Goodglass and Kaplan, 1971; Metz-Lutz et al., 1991]. Visual field, visual functions, and eye movements were monitored as previously described by Gras-Combe et al. (2012). The screen was divided in four virtual quadrants with a cross in the center. Two different pictures (from DO 80) were presented together, the former in the visual quadrant subserved by the OR fibers that the neurosurgeon expected to encounter during the resection, the latter in the opposite visual quadrant. The patients were asked to name the pictures staring at the center of the screen and the neuropsychologist collected the functional response errors (flashes, phosphenes, blurred vision, shadows, agnosia) and eventual spontaneous saccades. The spatial cognition was assessed with a line bisection task, according to the technique previously described [Bartolomeo et al., 2007; Thiebaut de Schotten et al., 2005]. Patients and neuropsychologist were not informed regarding the timing of DES during the execution of the different tasks. According to the technique described by Ojemann et al. (1989), each cortical or subcortical point was considered crucial for functional execution and was stored with numerical tags when its stimulation induced disturbances during three trials, as previously reported [Duffau et al., 2005; Duffau, 2009; Ius et al., 2011]. The different functional response errors collected during surgery were separately stored and associated with a specific numerical tag.

Functional Response Errors Collection

All patients underwent preoperative and postoperative (3-months) volumetric high-resolution T1-weighted axial sequences (slice thickness 1 mm; no interslice gap; FOV 280 mm; 1.5 T scanner) with gadolinium. All the postoperative T1 MRIs were used for the volumetric segmentation of residual tumours and surgical cavities with the freeware Osirix Imaging Software (http://www.osirix-viewer.com/). All the ROIs of residuals and surgical cavities were manually drawn on each axial slice and then exported for the elaboration of the atlas by the first author (S.S.) who is a neurosurgeon expert in brain anatomy, WM dissection, surgical treatment of brain tumours and medical imaging. The functional points, identified during intraoperative DES and stored with detailed high-resolution pictures, were included in the axial volumetric T1 by the first author (S.S.) comparing the anatomical landmarks of the single picture with the axial volumetric T1 and the reformatted sagittal and coronal sequences oriented according to the intraoperative lateral position of the head. Each functional response was saved and exported as a circular ROI with 0.2 cm^2 of total area. We collected 339 functional response errors (mean per patient: 2.6; SD: 1.2): 43 (AF) phonological and 61 (IFOF) semantic paraphasias, 6 reading disturbances, 75 motor and 43 somato-sensorial responses, 12 motor and language perseverations, 3 eyes apraxias, 13 visual disturbances, 9 spatial perception and 15 motor planning deficits, 25 verbal apraxias, 12 pure anomias, 22 speech arrests. All the functional response errors, classified by a specific color code and resumed in the same 3D MNI brain reconstruction, are showed in Figure 1. In Supporting Information Table SI, we provided the MNI coordinates of all functional response errors collected.

Creation of the Subcortical Functional Atlas and Resection Probability Map

Volumetric high-resolution T1-weighted axial sequences (slice thickness 1 mm; no interslice gap; FOV 28 mm; 1.5 T scanner) of all patients were spatially registered to the MNI space, $1mm^3$ voxel spatial resolution [Evans et al., 1992]. Nonbrain material was first removed from the T1-images using FSL's brain extraction tool (BET; FSL software available at http://www.fmrib.ox.ac.uk/fsl). Registration of resulting images was performed by applying 12 parameter affine transformations using FSL's linear image registration tool (FLIRT). Resulting registration models were subsequently used to spatially co-register ROIs of residuals, surgical cavities and functional points of all patients. Results were systematically assessed by visual inspection. All the statistical analyses were performed in the R Statistical Package (available at http://www.r-project.org; library Rniftilib was used for data import/export).

Let $\{x_i\}_{i=1,\ldots,N}$ be the set of the barycenter position of the $N = 339$ functional response errors coregistered to the MNI space and let us consider a certain functional response error R. We assume that a function $f(x)$ exists, defined for each voxel x of the brain in the MNI space and taking values between 0 and 1 proportionally to the probability that voxel x is associated with the functional response error R. Standard kernel regression techniques are used to approximate f: specifically, we define the approximation as $f_h(x) = 1-e^{-F_h(x)}$ where $F_h(x) = \sum_{i=1}^{N} K_h(x, x_i) y_i$ is a kernel regressor with Gaussian kernel $K_h(x, x_i) = e^{-\|x-x_i\|^2/2h^2}$ (depending on the kernel bandwidth h, controlling the spreading of the probability mass around a pointx_i) and $y_{i=1}$ if x_i is a voxel associated with the functional response error R, and 0 otherwise. Such approximation is supported

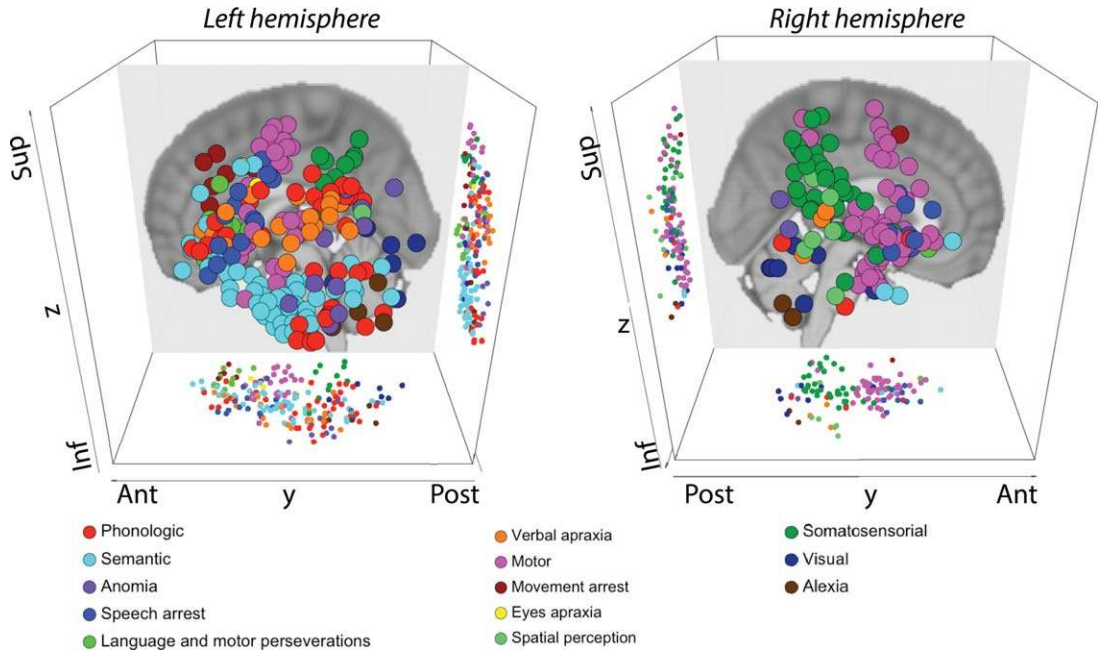

Figure 1.

3D representation of functional response errors collected with subcortical DES in the left and right hemispheres. Different colors represent the different functional response errors. The small colored points represent the projections of functional response errors on the *x*–*y* and *x*–*z* planes of the MNI space. DES: direct electrical stimulation; MNI: Montreal Neurological Institute. [Color figure can be viewed in the online issue, which is available at wileyonlinelibrary.com.]

by the fact that the Gaussian kernel takes value 1 in voxels x_i associated with the function response error R and values close to 1 in nearby regions (depending on h). Consequently, in regions at high density of functional response errors R function F_h takes large values. When the number of functional response errors is very large F_h diverges to ∞ and thus the function f_h tends to 1. Following the same line of reasoning, it is easy to see that f_h tends to 0 in regions empty of functional response errors R. The kernel bandwidth h was optimised by minimizing the error functional $\int (f - f_h)^2 dx$, approximated by leave one out cross-validation, a statistical technique aimed at estimating the prediction error of a model. More in detail, an instance of the prediction error can be obtained by using a single observation for error estimation and the remaining data for model development; the leave one out cross-validation error is obtained by averaging the prediction error over all observations. The above described procedure was used to approximate function f and to produce statistical maps in the MNI space for all functional response errors considered in this study. We found that the optimal value of the bandwidth varies from 4 mm to 5 mm for all considered functional response errors, which is coherent with the diameter of the employed bipolar electrode.

Let $M = \{(x_i, y_i, z_i, p_i)\}_{i=1,\ldots,n}$ be a certain ROI where (x_i, y_i, z_i) represent coordinates in the MNI space and p_i represent probability levels associated to voxels. We define the probabilistic center of mass of the ROI as the point of the MNI space of coordinates $x = \sum_{i=1,\ldots,n} x_i p_i / \sum_{i=1,\ldots,n} p_i$, $y = \sum_{i=1,\ldots,n} y_i p_i / \sum_{i=1,\ldots,n} p_i$ and $z = \sum_{i=1,\ldots,n} z_i p_i / \sum_{i=1,\ldots,n} p_i$. The B-distance between two ROIs is defined as the Euclidean distance between the centres of mass of the two ROIs. This allowed us to measure the distance between statistical maps in the MNI space for all functional response errors considered in this study (functions f_h defined above) and the bundles available in the DTI Atlas from Thiebaut de Schotten et al. (2011). When more than one bundle matched with the spatial distribution of the statistical map of a functional response error, we performed a χ^2 test in order to assess statistical significant differences ($P < 0.05$) in terms of distance between functional response errors and the different bundles.

The spatial distribution of functional response errors identified by DES defines clear resection limits. To characterize these limits for each bundle included in the DTI Atlas from Thiebaut de Schotten et al. (2011) and region of the AAL Atlas [Tzourio-Mazoyer N et al., 2002] two indicators were used, aimed at quantifying the nonresection probability and the resected volume of each ROI, and aimed at identifying differentially preserved regions within each ROI.

Specifically, the non resection probability (NRP) of a ROI was defined as the weighted average of the volume of

the non resected tumor invading the ROI divided by the overall volume of the tumor invading the ROI; the resection volume percentage (RVP) of a ROI was defined as the weighted average of the resected volume of the tumour invading the ROI divided by the volume of the ROI. These two indicators are measured in voxels. More formally, let us consider a certain region of interest G (a bundle or a AAL region), of volume $V_{G,}$ and let p be a patient. Let T_p be the volume of the tumor affecting patient p restricted to region G, and let R_p be the volume of the resected tumor restricted to region G. The NRP of the region G for patient p is defined as $x_p = (T_p - R_p)/T_p$ and the resection volume of the region G for patient p is defined as $y_p = T_p/V_G$. The NRP index is thus defined as $\sum_p t_p x_p$, where $t_p = T_p/\sum_p T_p$and the RVP index is defined as $\sum_p t_p y_p$. Weighted averages are more appropriate in this case as patient's tumors invading bundles/AAL regions are not homogeneous in size. Indeed, we adopted the above definition to make NRP and RVP more influenced by tumors invading large portions of the region of interest G (it is easy to check that, for instance, the contribution of patient p to the computation of NRP and RVP is negligible if T_p is small compared to tumors of other patients). Statistical difference between the left/right nonresection probabilities $\{x_p\}$ and left/right resection volumes $\{y_p\}$ was assessed by means of a weighted Student's t-test (wtd.t.test function of the package "weights" of the R statistical package) and coefficients t_p were used as weights. To identify differentially preserved regions of each bundle/AAL region we adopted the following procedure: let us consider a voxel x of the brain in the MNI space. The co-registered ROIs of residuals and surgical cavities allow us to compute the number $n(x)$ of times voxel x is part of a lesion region (either resected or not) and the number $r(x)$ of times voxel x has been resected. The probability of nonresectability is defined as $p(x) = (n(x) - r(x))/n(x)$ and, by assuming that $p(x)$ is binomial distributed$B(n(x), n(x) - r(x))$, 95% confidence intervals can be computed through exact binomial test. The above described procedure was used to produce a statistical map (with 95% CI) of nonresectability in the MNI space.

RESULTS

Surgical Cavities and Tumour Residues

The mean preoperative volume of the tumours was 67.3 cc (SD: 39.7). In 78 cases, the tumour invaded the WM of the frontal lobe, in 63 the temporal lobe, in 45 the insular lobe and the WM of the external capsule (EC), the parietal lobe in 17 cases and in 5 cases the occipital lobe. In 56 cases, the tumours involved the WM of more than 1 lobe and in 24 cases three lobes. Among the 12 left-handed patients, 7 underwent resection of lesions within the right hemisphere and 5 within the left; 6 ambidextrous patients were operated on the right and 1 on the left side; all right-handed patients were operated for a left lesion. According to intraoperative DES, eloquent language response errors were reported: in the left hemisphere in all the 111 right-handed patients; in the right hemisphere in 1 left-handed patient (14.3%) between the 7 tested on this side; in the right hemisphere in 3 (50%) of ambidextrous patients between the 6 tested on this side and in the left hemisphere in the sole ambidextrous patient operated on the left side.

Transient postoperative immediate mild to moderate deficits were reported in 39 patients (30%). At 3-months follow-up, all patients recovered and no permanent impairments with respect to the preoperative tests was reported. The mean resection rate was 90.8% and the mean residual tumour was 6.2 cc (SD: 4).

Anatomical Analysis of Distribution of Functionally Critical WM According to DES

The executive motor functions were distributed in the central region and within the vertical projection fibers of the cortico-spinal tract (CST) directed up to the internal capsule (IC). The functional response errors for motor planning (corresponding to movement arrest, eyes apraxia, language, and motor perseverations) were localized in the dorso-medial portion of the frontal WM with an oblique course, connecting the deep nuclei (i.e. the caudate nucleus) to the superior frontal cortices [particularly the supplementary motor area (SMA) and pre-SMA] (Figs. 2a–c; 3b). The speech planning (corresponding to the speech arrest) identified tracts strongly localized in the most ventral and lateral portion of the frontal WM, corresponding to the fibers terminating in the ventral premotor cortex (VPMC) (Fig. 3a). The somato-sensorial functional responses were localized in the postcentral region and within the vertical fibers projecting to the posterior portion of the internal capsule (IC) (Fig. 4a).

The phonological language response errors were distributed within the ventral and lateral WM of the frontal lobe, in the lateral and inferior WM of the parietal lobe and in the posterior and middle thirds of the superior temporal gyrus (STG), middle temporal gyrus (MTG), and inferior temporal gyrus (ITG), with a "C" shaped course running around the insula outside from the external capsule (EC) and temporal stem (TS) (Fig. 5a). Verbal apraxia deficits were distributed with a horizontal course from the VPMCs in a direct posterior direction up to the inferior parietal lobule (IPL) with a more lateral distribution with respect to the phonologic response errors (Fig. 3c). Semantic paraphasias were distributed within the most ventral and medial WM of the temporo-parietal junction, in the medial WM of the temporal lobe over the roof of the temporal horn of the lateral ventricle, in the ventral portion of the EC and within the WM of the frontal lobe with a more superior and anterior direction up to the middle and posterior thirds of the middle frontal gyrus (MFG), superior frontal gyrus (SFG), and to the ventral cortices of the

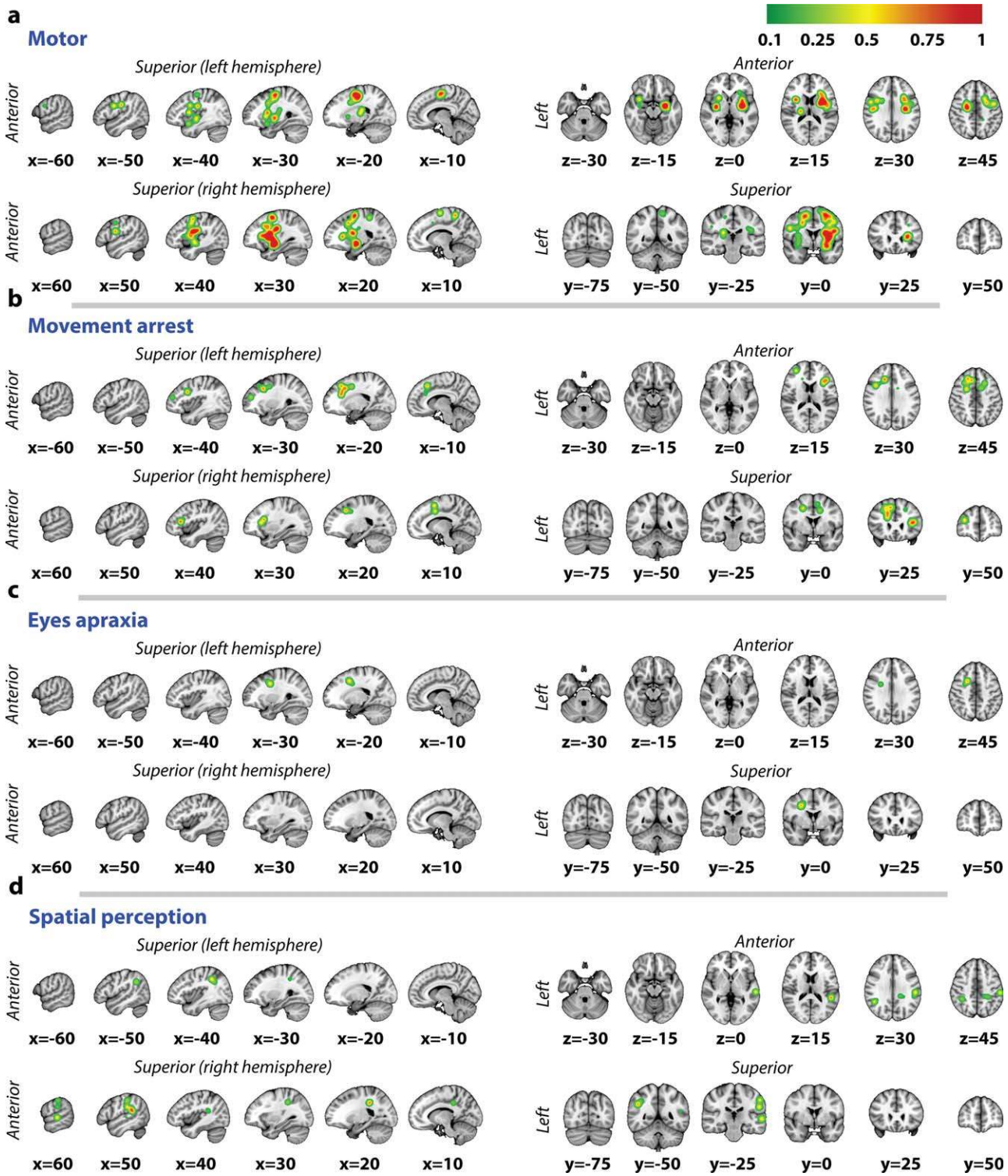

Figure 2.

Spatial distribution of the functional response errors related to motor execution (**a**), movement arrest (**b**), eyes apraxia (**c**), and spatial perception (**d**) (functions $f_h(x)$described in Material and Methods) in the MNI space coordinates (in mm). Green to red colours represent increasing levels of probability (color scale on the right top). In the left column, the eloquent response errors are reported within the left and right hemispheres (superior and inferior raw, respectively). In the right column the eloquent sites are shown on the axial plane (superior raw) and on the coronal plane (inferior raw). Negative to positive *x* coordinates scroll from the left to the right hemisphere on the sagittal plane; negative to positive *z* coordinates scroll from the inferior to the superior regions on the axial plane; negative to positive *y* coordinates scroll from the posterior to the anterior regions on the coronal plane. MNI: Montreal Neurological Institute. [Color figure can be viewed in the online issue, which is available at wileyonlinelibrary.com.]

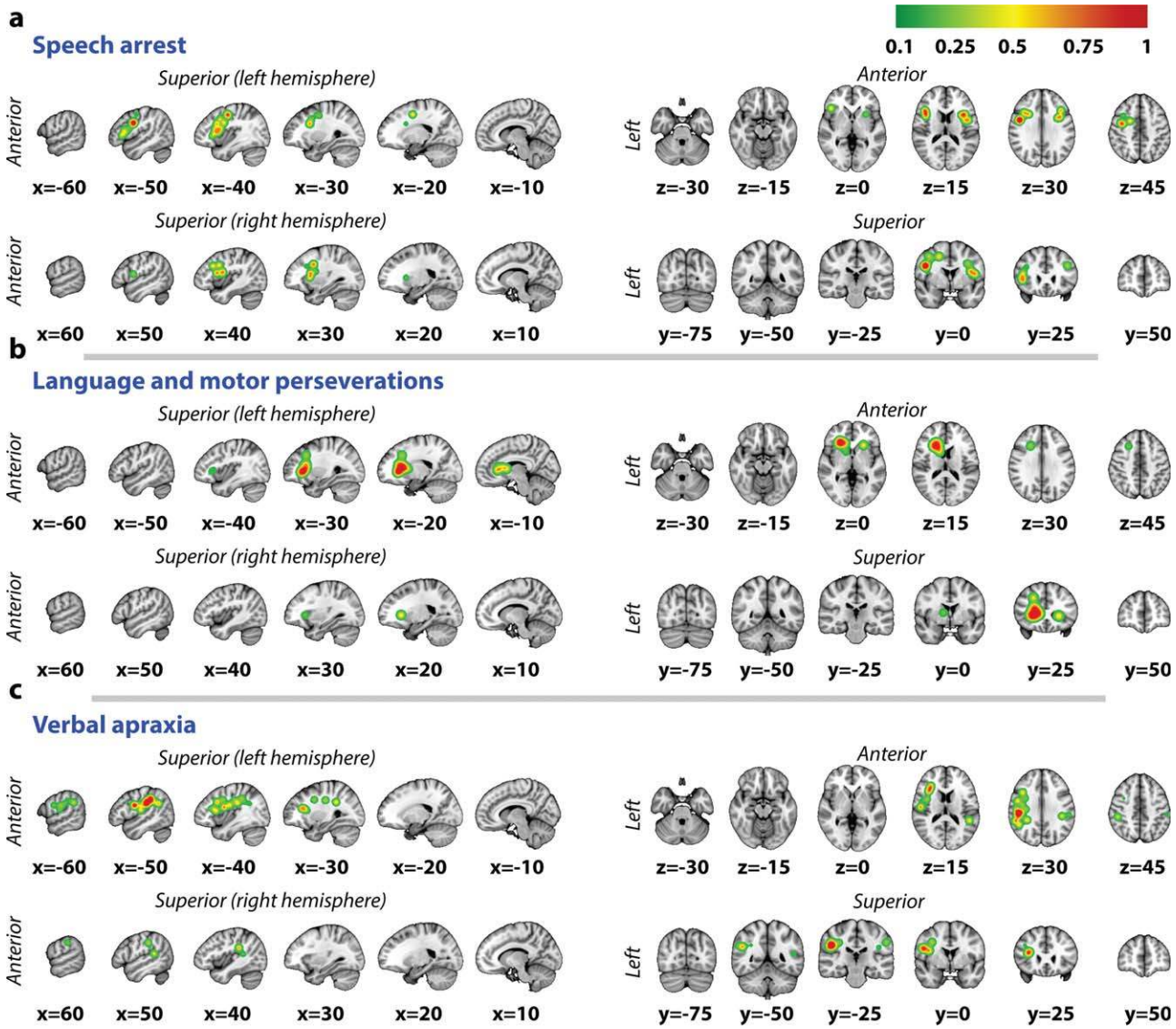

Figure 3.

Spatial distribution of the subcortical eloquent sites regarding speech arrest (**a**), language/motor perseverations (**b**), and verbal apraxia (**c**) (functions $f_h(x)$ described in Material and Methods) in the MNI space coordinates (in mm). Green to red colors represent increasing levels of probability (color scale on the right top). In the left column, the eloquent response errors are reported within the left and right hemispheres (superior and inferior raw, respectively). In the right column, the eloquent sites are shown on the axial plane (superior raw) and on the coronal plane (inferior raw). Negative to positive *x* coordinates scroll from the left to the right hemisphere on the sagittal plane; negative to positive *z* coordinates scroll from the inferior to the superior regions on the axial plane; negative to positive *y* coordinates scroll from the posterior to the anterior regions on the coronal plane. MNI: Montreal Neurological Institute. [Color figure can be viewed in the online issue, which is available at wileyonlinelibrary.com.]

inferior frontal gyrus (IFG) (Fig. 5b). Reading deficits were localized with an antero-inferior course in the lateral long WM of the occipital and temporal lobe (Fig. 4c).

The WM of the temporal stem (including claustro-opercular and insulo-opercular fibers of the external and extreme capsules, the auditory radiations, IFOF, UF, OR, anterior commissure, and inferior thalamic peduncle) of the right hemisphere was more frequently resectable in respect to the contralateral hemisphere where the residual threshold is highest (Fig. 6a–c). On the other hand, the

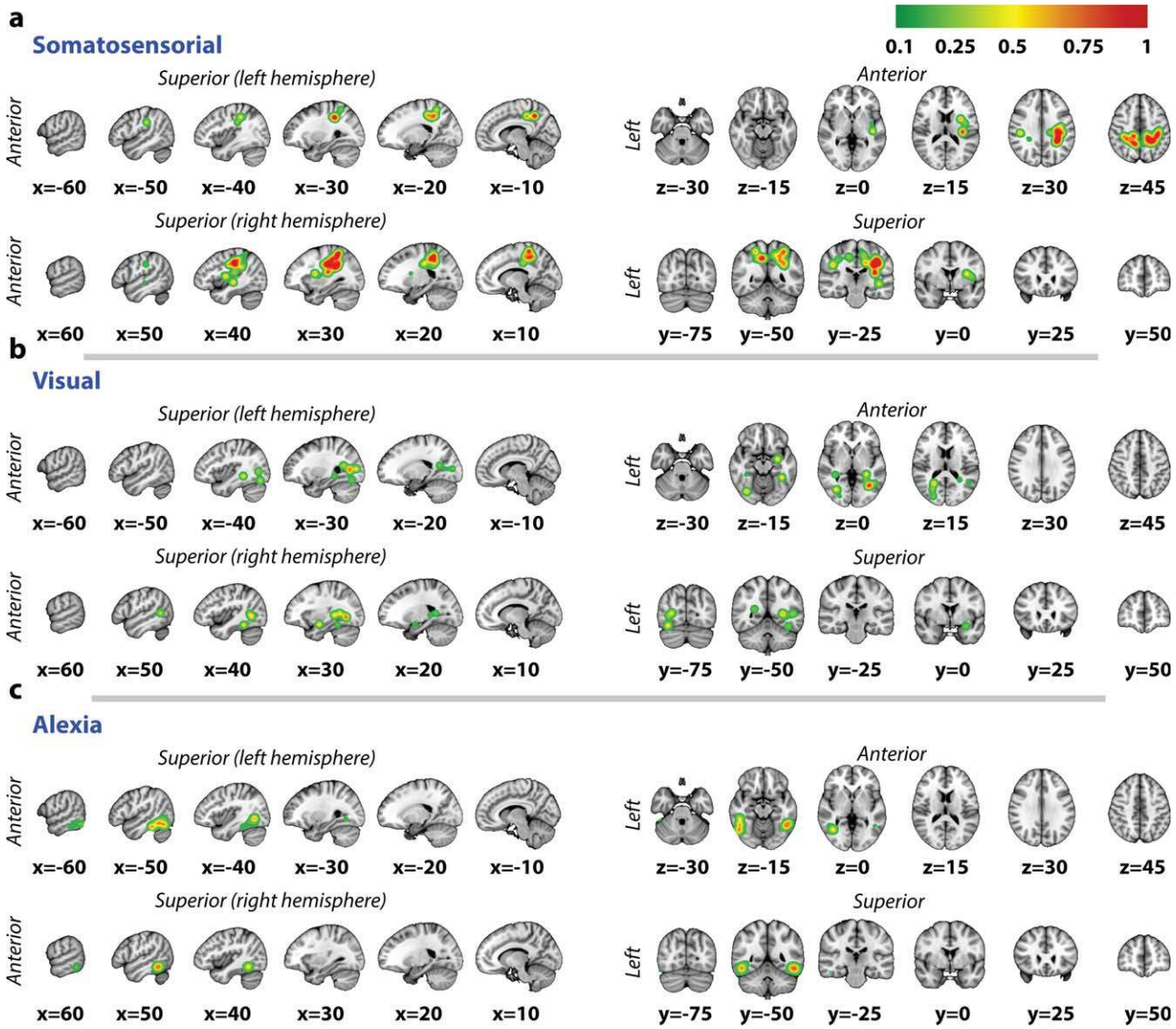

Figure 4.

Spatial distribution of the response errors regarding somatosensorial (**a**), visual (**b**), and reading (**c**) functions (functions $f_h(x)$ described in Material and Methods) in the MNI space coordinates (in mm). Green to red colors represent increasing levels of probability (color scale on the right top). In the left column, the eloquent response errors are reported within the left and right hemispheres (superior and inferior raw, respectively). In the right column, the eloquent sites are shown on the axial plane (superior raw) and on the coronal plane (inferior raw). Negative to positive *x* coordinates scroll from the left to the right hemisphere on the sagittal plane; negative to positive z coordinates scroll from the inferior to the superior regions on the axial plane; negative to positive *y* coordinates scroll from the posterior to the anterior regions on the coronal plane. MNI: Montreal Neurological Institute. [Color figure can be viewed in the online issue, which is available at wileyonlinelibrary.com.]

WM of the central region, corresponding to the projection of motor and sensory pathways from the M1 and S1 was not resectable with approximately the same probability on both sides. The more ventral and horizontal connections between the frontal and parietal lobes (corresponding to the lateral indirect anterior portion of the SLF and AF), just lateral with respect to the projection CST and CTT, are more frequently preserved on the left side (Fig. 6a–c). On the right side, instead, the more dorsal horizontal WM connecting the dorsal superior frontal gyrus to the parietal

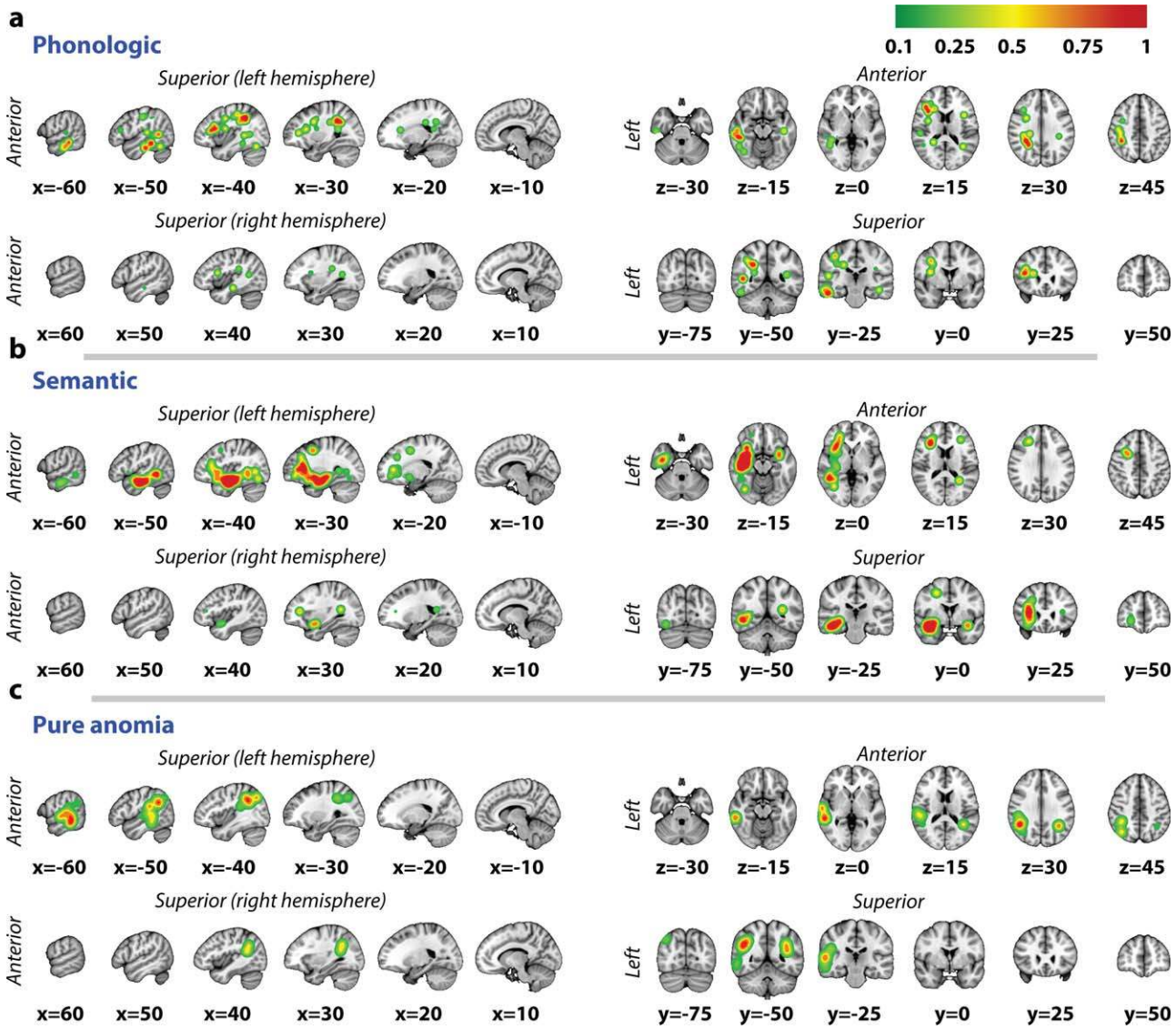

Figure 5.

Subcortical spatial distribution of the phonological (**a**) and semantic paraphasias (**b**) as well as pure anomias (**c**) (functions $f_h(x)$ described in Material and Methods) in the MNI space coordinates (in mm). Green to red colors represent increasing levels of probability (color scale on the right top). In the left column, the eloquent response errors are reported within the left and right hemispheres (superior and inferior raw, respectively). In the right column, the eloquent sites are shown on the axial plane (superior raw) and on the coronal plane (inferior raw). Negative to positive *x* coordinates scroll from the left to the right hemisphere on the sagittal plane; negative to positive *z* coordinates scroll from the inferior to the superior regions on the axial plane; negative to positive *y* coordinates scroll from the posterior to the anterior regions on the coronal plane. MNI: Montreal Neurological Institute. [Color figure can be viewed in the online issue, which is available at wileyonlinelibrary.com.]

lobe and to the deep nuclei (i.e. caudate nucleus) is more frequently preserved because of functional responses at DES (Fig. 6a–c). These regions correspond to the course of the SCF or anterior third of the cingulum (Cing) fibers. The most medial WM of the occipital and temporal lobes were crucial for language and visual functions on both sides, corresponding to the course of the IFOF and OR (Figs. 4b,c; 5b).

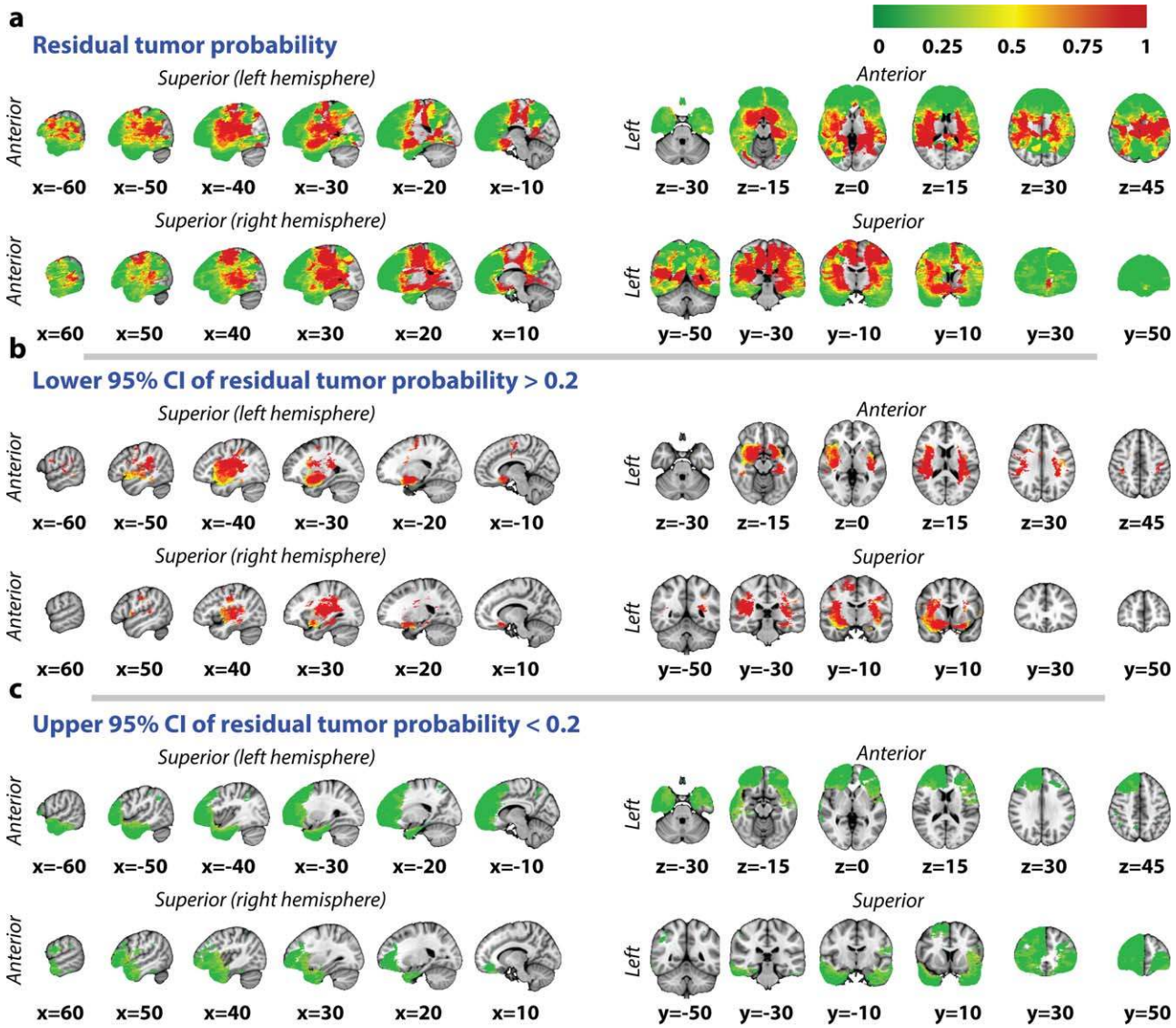

Figure 6.

In panel (a), we collected the sagittal, coronal and axial views of the statistical map of the NRP [function *p(x)* described in Material and Methods with the respective colour scale on the right top] in the MNI space coordinates (in mm). In panels (b) and (c), we included also the regions with the highest statistical significance (lower 95% CI of residual tumor probability > 0.2 and upper 95% CI of residual tumor probability < 0.2, respectively), considering that the statistical significance of the map depends on the number of tumors per voxel and is not spatially homogenous. Negative to positive *x* coordinates scroll from the left to the right hemisphere on the sagittal plane; negative to positive *z* coordinates scroll from the inferior to the superior regions on the axial plane; negative to positive *y* coordinates scroll from the posterior to the anterior regions on the coronal plane. MNI: Montreal Neurological Institute; NRP: non-resection probability. [Color figure can be viewed in the online issue, which is available at wileyonlinelibrary.com.]

DTI Analysis of the Functions Distribution and Residual WM

The analysis concerning the NRP demonstrated an asymmetry between the left and right hemisphere in the resection rate of AF, the lateral indirect anterior portion of SLF, the lateral posterior portion of the indirect SLF, IFOF, and CST (NRP left/right side, respectively: 80/57%, $P = 0.001$; 90/58%, $P < 0.001$; 81/68%, $P = 0.02$; 47/58%, $P = 0.03$; 77/90% $P = 0.03$)(Figs. 5a–c; 6a–c). Similar resection rates were reported for OR, ILF, and UF (NRP left/right side, respectively: 89/84%, $P = 0.49$; 45/43%, $P = 0.85$; 52/39%, $P = 0.1$) (Table I).

TABLE I. In this table, we summarized the difference in NRP (including the *P* values) between the left and the right hemisphere for the white matter tracts considered

Fascicle	Left (%)	Right (%)	*P*
AF	80	57	0.001
A/I SLF	90	58	<0.001
P/I SLF	81	68	0.02
IFOF	47	58	0.03
CST	77	90	0.03
OR	89	84	0.49
ILF	45	43	0.85
UF	52	39	0.1

AF: arcuate fascicle; A/I SLF: Anterior indirect component of superior longitudinal fascicle; CST: cortico-spinal; IFOF: inferior fronto-occipital fascicle; ILF: inferior longitudinal fascicle; NRP: non-resection probability index; OR: optic radiation; UF: Uncinate fascicule; P/I SLF: Posterior indirect component of superior longitudinal fascicle.

Above results were confirmed from the statistical analysis of the RVP of each bundle, which resulted to be highly anticorrelated with NRP (Spearman rank correlation: $r = -0.79$, $P < 0.001$). Specifically, we found that the resected volume of AF, lateral indirect anterior and posterior portion of SLF, IFOF, CST, OR, ILF, and UF were on the left/right side, respectively: 6/14% ($P = 0.001$), 6/25% ($P = 0.001$), 5/19% ($P = 0.01$), 15/8% ($P < 0.001$), 2/1% ($P = 0.01$), 3/4% ($P = 0.82$), 17/16% ($P = 0.65$), 26/29% ($P = 0.46$).

The matching analysis between the functional response errors elicited by DES during surgery and the bundles available in the DTI Atlas from Thiebaut de Schotten et al. (2011) demonstrated that:

1. The spatial distribution of motor responses matches with the spatial distribution of the cortico-spinal and cortico-thalamic fibers (B-distance 17.7mm, Fig. 7a), the indirect anterior portion of the SLF (B-distance

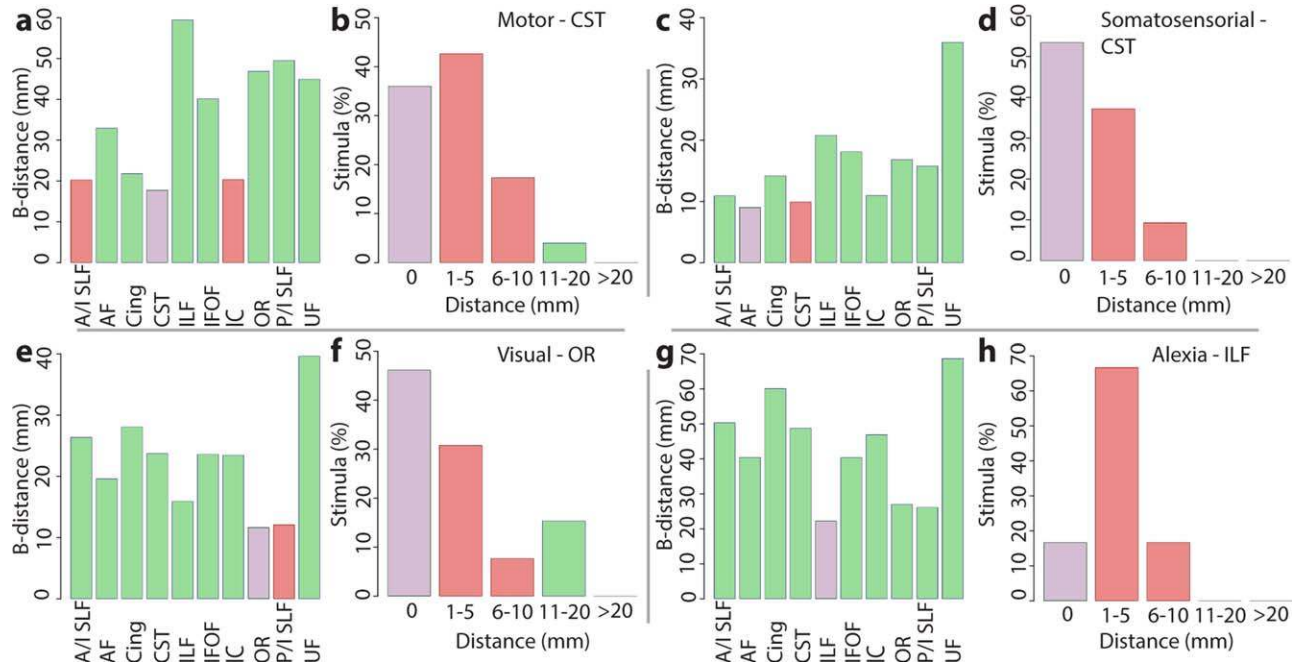

Figure 7.

(**a**) B-distance (the distance between the probabilistic centers of mass, see Material and Methods) between the spatial distribution of functional responses related to motor execution and bundles of the Thiebaut de Schotten et al. (2011) probabilistic Atlas. Violet identifies the bundle at minimal B-distance. Red identifies bundles at distance lower than 120% of minimal B-distance. Bundles at larger B-distance are shown in green. (**b**) Distribution of the distances (in mm) of motor responses collected during surgeries from the CST. The distance between a functional point and a bundle is defined as the minimal distance between all voxels of the functional response and all voxels of the bundle. It is set to 0 when functional response and bundle intersect. (**c**) As (a) but for somato-sensorial responses. (**d**) As (b) but for the distance of somato-sensorial responses from the CST. (**e**) As (a) but for visual response errors. (**f**) As (b) but for the distance of visual response errors from the OR. (**g**) As (a) but for alexias. (**h**) As (b) but for the distance of alexias from the ILF.A/I SLF: Anterior indirect component of superior longitudinal fascicle; Cing: Cingulum; AF: arcuate fascicle; CST: cortico-spinal; IFOF: inferior fronto-occipital fascicle; ILF: inferior longitudinal fascicle; OR: optic radiation; IC: internal capsule; UF: Uncinate fascicule; P/I SLF: Posterior indirect component of superior longitudinal fascicle. [Color figure can be viewed in the online issue, which is available at wileyonlinelibrary.com.]

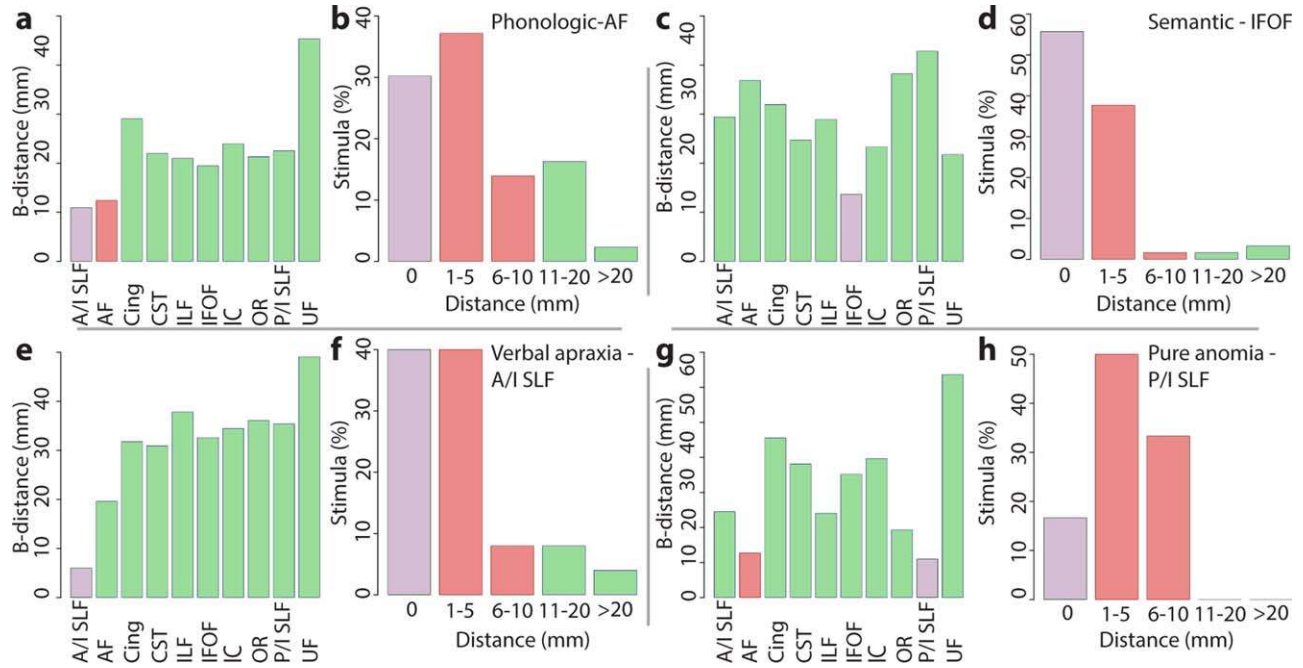

Figure 8.

(**a**) B-distance (the distance between the probabilistic centers of mass, see Material and Methods) between the spatial distribution of phonological functional response errors and bundles of the Thiebaut de Schotten et al. (2011) Atlas. Violet identifies the bundle at minimal B-distance. Red identifies bundles at distance lower than 120% of minimal B-distance. Bundles at larger B-distance are shown in green. (**b**) Distribution of the distances (in mm) of phonological response errors collected during surgeries from AF. The distance between a functional point and a bundle is defined as the minimal distance between all voxels of the functional response and all voxels of the bundle. It is set to 0 when functional response and bundle intersect. (**c**) As (a) but for semantic paraphasias. (**d**) As (b) but for the distance of semantic paraphasias from the IFOF. (**e**) As (a) but for verbal apraxias. (**f**) As (b) but for the distance of verbal apraxias from the Anterior/Indirect component of SLF. (**g**) As (a) but for pure anomias. (**h**) As (b) but for the distance of pure anomias from the Posterior/Indirect component of SLF.A/I SLF: Anterior indirect component of superior longitudinal fascicle; Cing: Cingulum; AF: arcuate fascicle; CST: cortico-spinal; IFOF: inferior fronto-occipital fascicle; ILF: inferior longitudinal fascicle; OR: optic radiation; IC: internal capsule; UF: Uncinate fascicule; P/I SLF: Posterior indirect component of superior longitudinal fascicle. [Color figure can be viewed in the online issue, which is available at wileyonlinelibrary.com.]

20.2 mm, Fig. 7a) and IC (B-distance 20.3 mm, Fig. 7a). However, 96% (72/75) of the motor responses were located within 1 cm from the cortico-spinal and cortico-thalamic fibers (Fig. 7b), while only 48% (36/75) were located within 1 cm from indirect anterior portion of the SLF and the difference is statistically significant ($\chi^2 = 40.5$; $P < 0.001$).

2. The spatial distribution of the sensory responses matches with the spatial distribution of the AF (B-distance 18.0 mm, Fig. 7c) and cortico-spinal and cortico-thalamic fibers (B-distance 19.8 mm, Fig. 7c). However, 100% (43/43) of sensory responses were located within 1 cm from the cortico-spinal and cortico-thalamic fibers (Fig. 7d) while only 74.4% (32/43) responses were located within 1 cm from the AF and the difference is statistically significant ($\chi^2 = 10.4$; $P = 0.001$).
3. The spatial distribution of the phonological deficits matches with the spatial distribution of the indirect anterior portion of the SLF (B-distance 10.9 mm, Fig. 8a) and the AF (B-distance 12.4 mm, Fig. 8a). However, 81.4% (35/43) of phonological deficits were located within 1 cm from the AF (Fig. 8b) while only 46.5% (20/43) of phonological deficits were located within 1 cm from the indirect anterior portion of the SLF and the difference is statistically significant ($\chi^2 = 9.9$; $P = 0.002$).
4. The spatial distribution of the semantic paraphasias matches consistently only with the spatial distribution of the IFOF (B-distance 13.7 mm, Fig. 8c). Moreover, 91.8% (56/61) semantic paraphasias were located within 1 cm from the IFOF (Fig. 8d).
5. The spatial distribution of verbal apraxia deficits matches consistently only with the spatial distribution of the indirect anterior portion of the SLF

(B-distance 6.0 mm, Fig. 8e). Moreover, 88% (22/25) of verbal apraxia deficits were reported within 1 cm from the indirect anterior portion of the SLF (Fig. 8f).

6. The spatial distribution of the pure anomia matches with the spatial distribution of the indirect posterior portion of the SLF (B-distance 11.0 mm, Fig. 8g) and the AF (B-distance 12.7 mm, Fig. 8g). 100% (12/12) of pure anomia were located within 1 cm from both the indirect posterior portion of the SLF (Fig. 8h) and the AF.
7. The spatial distribution of the visual response errors (positive: flashes, phosphenes; negative: agnosia) matches with the spatial distribution of the OR (B-distance 23.3 mm, Fig. 7e) and the indirect posterior portion of the SLF (B-distance 24.2 mm, Fig. 7e). However, 84.6% (11/13) of visual response errors were located within 1 cm from the OR (Fig. 7f) while only 53.8% (7/13) response errors were located within 1 cm from the indirect posterior portion of the SLF ($\chi^2 = 1.6$; $P = 0.20$). 84.6% (11/13) of visual response errors were located within 1 cm from the IFOF.
8. The spatial distribution of alexia matches consistently only with the spatial distribution of the ILF (B-distance 22.2 mm, Fig. 7g). Moreover, 100% (6/6) of alexia were located within 1 cm from the ILF (Fig. 7h).
9. The spatial distribution of spatial perception deficits matches mainly with the course of the AF (B-distance 7 mm). Moreover, 100% (9/9) of these functional response errors were elicited within 1 cm from the AF. The B-distance from SLF (indirect anterior component) is 16 mm.

For a complete analysis of the distance between functional response errors and bundles see also Supporting Information Table SI.

Cortical Analysis of the WM Terminations and Functional Response Errors

According to the analysis of the NRP on the AAL Atlas [Tzourio-Mazoyer et al., 2002], the more frequent and large resections were reported within the frontal and temporal lobe on both the sides. In the anterior regions of the frontal lobe, the WM terminating in the superior, middle and medial fronto-orbital gyri (SFOG, MidFOG, and MedFOG, respectively) and in the SFG and MFG were more frequently resected on both sides (NRP left/right side, respectively: 9/11%, $P = 0.73$; 3/6%, $P = 0.72$; 9/14%, $P = 0.63$; 7/17%, $P = 0.34$; 7/10%, $P = 0.59$). In the posterior regions of the frontal lobe, the WM directed to the precentalgyrus (PreCG), to the SMA, to the rolandic opercula (RolOp) and to the pars opercularis of the IFG (OpIFG) were less frequently resected (NRP left/right side, respectively: 73/71%, $P = 0.87$; 32/65%, $P = 0.002$; 76/49%, $P = 0.003$; 56/33%, $P = 0.008$), especially in the dorsal and medial portions of the posterior WM of the right frontal lobe and in the ventral portion on the left side (Fig. 5a,b). On the other hand, the WM terminating in the anterior two-thirds of the IFG, corresponding to the pars orbitalis and triangularis (OrbIFG and TrIFG, respectively), were frequently removed (NRP left/right side, respectively: 29/15%, $P = 0.38$; 17/12%, $P = 0.38$), with a mild prevalence on the right side.

The WM terminating within the superior and middle temporal pole (STP and MTP, respectively) and the ITG were the most frequently resected (NRP left/right side, respectively: 30/15%, $P = 0.06$; 4/7%, $P = 0.62$; 12/18%, $P = 0.32$). The most preserved fibers were terminating in the STG and MTG, respectively and in the amygdala, the hippocampus and the parahippocampus (NRP left/right side, respectively: 55/45%, $P = 0.22$; 24/32%, $P = 0.29$; 77/54%, $P = 0.02$; 52/56%, $P = 0.69$; 21/33%, $P = 0.26$).

The WM connecting the postcentral and para-central lobule (PostCL and ParaCL, respectively), the calcarine cortices, the mid and posterior portion of the Cing, the insula, the angular gyrus (AG), the supra-marginal gyrus (SMG), and the lingual gyrus were highly preserved (NRP left/right side, respectively: 58/53%, $P = 0.58$; 98/86%, $P = 0.2$; 86/99%, $P = 0.49$; 53/56%, $P = 0.69$; 28/41%, $P = 0.45$; 65/42%, $P = 0.001$; 47/29%, $P = 0.26$; 66/33%, $P < 0.001$). The regions more frequently resected within the occipital, parietal and temporal lobes were: precuneus, cuneus, the superior parietal cortices, IOG and middle occipital gyrus (MOG), the superior occipital gyrus (SOG) (NRP left/right side, respectively: 17/19%, $P = 0.84$; 30/31%, $P = 0.98$; 22/4%, $P = 0.22$; 22/2%, $P = 0.24$; 30/30%, $P = 0.97$; 6/40%, $P = 0.38$) (Table II).

The statistical analysis of the RVP of each region of the AAL Atlas shows that RVP is highly anticorrelated with NRP (Spearman rank correlation: $r = -0.81$, $P < 0.001$).

The anatomical analysis of the location of the functional response errors in respect to the cortical areas of the AAL Atlas demonstrated that: the phonological response errors are more frequently reported in the WM terminating in the frontal lobe (TrIFG 15.4%, MFG 10,3%, OpIFG 7.7,%, PreCG 5.1%, RolOp 2.6%) and temporal lobe (MTG 28.2%, ITG 23.1%, STG 5.1%, Fusiform 5.1%); the semantic response errors were more often observed in the WM terminating in the frontal lobe (TrIFG 11.7%, MFG 11.7%, SFG 3.3%, PreCG 1.7%, OrbSFG 1.7%; OrbMFG 1.7%); anomia were reported within the MTG, STG inferior parietal region, SMG, AG, ITG, MOG (respectively: 41,7%, 33.3%, 25%; 25%, 25%, 8.3%, 8.3%); the responses regarding the motor planning were exclusively reported in the WM terminating in the frontal lobe (movement arrest: SFG 71.4%; SMA 57.1%; SFG_medial 28.6%; antCing 28.6%; midCing 14.3%; language and motor perseverations: Caudate (Caud) 54.5%, Put 18.2%, TrIFG 27.3%, MFG 9.1%; SFG 9.1%); the response errors regarding the language planning were mostly found in the WM terminating in the ventral and posterior cortices of the frontal lobe

TABLE II. We report the differences in NRP (including *P* values) between left the right hemisphere for the cortical regions, according to the matching analysis with the AAL Atlas

Area	Left (%)	Right (%)	*P*
SFOG	9	11	0.73
MidFOG	3	6	0.72
MedFOG	9	14	0.63
SFG	7	17	0.34
MFG	7	10	0.59
PrecCG	73	71	0.87
SMA	32	65	0.002
RolOp	76	49	0.003
OpIFG	56	33	0.008
OrbIFG	29	15	0.38
TrIFG	17	12	0.38
STP	30	15	0.06
MTP	4	7	0.62
ITG	12	18	0.32
STG	55	45	0.22
MTG	24	32	0.29
Amygdala	77	54	0.02
Hippocampus	52	56	0.69
Parahippocampus	21	33	0.26
PostCL	58	53	0.58
ParaCL	98	86	0.2
Calc	86	99	0.49
Cingulum	53	56	0.69
Insula	28	41	0.45
AG	65	42	0.001
SMG	47	29	0.26
Lingual gyrus	66	33	0.001
Precuneus	17	19	0.84
Cuneus	30	31	0.98
Superior Parietal Cortices	22	4	0.22
IOG	22	2	0.24
MOG	30	30	0.97
SOG	6	40	0.38

AG: angular gyrus; Calc: calcarine cortices; Cing: cingulum; IFG: inferior frontal gyrus; IFOF: inferior fronto-occipital fascicle; IOG: inferior occipital gyrus; ITG: inferior temporal gyrus: MedFOG: medial fronto-orbital gyrus; MFG: middle frontal gyrus; MidFOG: middle fronto-orbital gyrus; MOG: middle occipital gyrus; MTG: middle temporal gyrus; MTP: middle temporal pole; NRP: non-resection probability; OpIFG: pars opercularis of inferior frontal gyrus; OrbIFG: pars orbitalis of inferior frontal gyrus; OrbMFG: orbital middle frontal gyrus; OrbSFG: orbital superior frontal gyrus; ParaCL: parac-central lobule; PreCG: pre-central gyrus; RolOP: rolandic opercula; PostCG: post-central gyrus; PostCL: post-central lobule; preSMA: pre-supplementary motor area; Put: putamen; SFG: superior frontal gyrus; SFOG: superior fronto-orbital gyrus; SMA: supplementary motor area; SMG: supra-marginal gyrus; SOG: superior occipital gyrus; SPL: superior parietal lobule; STG: superior temporal gyrus; STP: superior temporal pole; TrIFG: pars triangularis of inferior frontal gyrus; UF: uncinate fascicle.

(particularly, speech arrest: OpIFG 38.1%, PreCG 33.3%, TrIFG 23.8%, MFG 14.3%, RolOp 4.8%) and of the inferior parietal lobule (verbal apraxia: PreCG 26.1%, OpIFG 17.4%, RolOp 17.4%, TrIFG 17.4%; SMG 34.8%, PostCG 34.8%, AG 4.3%); errors concerning spatial awareness were elicited within the parietal lobe (SMG 44.4%, PostCG 33.3%, IPL 11,1%, AG 11.1%) up to the junction with the temporal lobe (STG 33.3%).

DISCUSSION

General Overview

DES is a reliable method for the direct identification of the eloquent cortical and subcortical regions of the brain. This technique provides reliable and accurate data regarding the specific functions subserved by the anatomical structure stimulated. Here, we used DES in a large population to provide, for the first time to our knowledge, an atlas summarizing the distribution of the essential sensorimotor, language and visual functions within the human WM.

Ius et al. (2011) first reported a systematic analysis of extensive resections in 55 patients who underwent awake surgery for LGGs, confirming the reliability of probabilistic brain atlases by means of spatial normalization of individual MRI scans and providing original data about the potential resectability of cortical and subcortical regions. In the present work, we adopted a similar methodology for the atlas computation to study a larger population with different aims. The distribution of the functional response errors collected with DES was integrated with anatomical data provided by DTI and cortical atlases providing the subcortical distribution of WM functions in both the left and right hemisphere.

The pure anatomical analysis demonstrated that larger brain regions are resectable without permanent *sequelae* within the right hemisphere, namely the ventral cortico-subcortical portion of the frontal lobe and the anterior, mid and dorso-lateral portion of the temporal lobe (Fig. 6a–c). On the contrary, the ventral cortices and WM of the frontal lobe as well as WM terminating in the posterior and dorso-lateral portion of the temporal lobe are crucial for many aspects of language elaboration within the left hemisphere (Figs. 3a–c; 5a–c). On the other hand, the postero-dorsal portion of the frontal lobe and ventro-medial portion of the temporal lobe were critical for motor elaboration and executive aspects, and for visual perception, respectively (Figs. 2a–c; 4b,c). The analysis of resected cortical areas and the distribution of the functional response errors in the subcortical regions revealed that the parietal lobe were critical in both hemispheres. Especially, the dorsal portion [i.e. superior parietal lobule (SPL)] in the right and the ventral region (i.e. IPL) in the left hemisphere, were crucially related to visuo-spatial functions and to different aspects of language elaboration, respectively (Figs. 2d; 5a–c). Portions of the insular region are frequently preserved with a significant difference between the left and right side, confirming this lobe as a real

neurosurgical challenge (at least for complete resections) for anatomical and functional reasons [Duffau, 2009].

Interestingly, our data demonstrate that the resectability rate of the subcortical eloquent WM is consistently lower in respect to cortical territories, which were more frequently resectable even if classically considered high-eloquent regions within both hemispheres. This is in agreement with our previous report on the minimal common brain [Ius et al., 2011]. Remarkably, even if the terminal portions of all main associative bundles analyzed were resectable, the other components of the tracts were crucial for the functional processing in all patients, with some variability. We did not report, in fact, bundles completely resectable in both the NRP and RVP analysis. These results support the crucial role of the associative connectivity in subserving the plastic anatomo-functional reorganization of the cortical territory to compensate brain damages, as demonstrated by DES and fMRI studies for different large, distributed and parallel networks [Duffau et al., 2003a, 2003b; Krainik et al., 2004; Sarubbo et al., 2012a, 2012b]. However, the statistical analysis demonstrated that some bundles present a significant difference in both NRP and RVP between left and right side. Bundles involved in language elaboration (AF, indirect lateral anterior and posterior portions of the SLF) are significantly less resected in the left side. No differences in the NRP and RVP of the ILF and OR, which resulted the second less resected bundle, were reported. On the other hand, the WM originating and terminating in the central and postcentral regions (i.e. the projection fibers of the CST and the CTT) in both hemispheres is characterized by the maximal NRP and minimal RVP. This is probably due to the fact that these connections have a role not in the functional integration, but rather in the transmission of the final functional output/input [Ius et al., 2011].

Functional Considerations and Atlas Description

We analyzed the anatomical distribution of the functional response errors within the subcortical WM. In order to understand a possible involvement of specific bundles in the networks explored during surgery, we also analyzed the possible matching of the overall subcortical distribution of different functional response errors with the bundles' reconstruction from Thiebaut de Schotten et al (2011). According to themodern connectomicperspective of the anatomo-functional organization of the CNS, the goal of this study is not to provide one-to-one relationships between bundles and functions, nor to claim that a single bundle could rigidly subserve one eloquent network. Quite the contrary, the aim is to understand a possible functional role of different bundles in specific aspects of neurological processing, according to the hypotheses previously reported in literature.

The results collected during repetition and counting tasks by stimulating the lateral and the ventral portion of the WM connecting the parietal and the temporal cortices to the frontal lobe demonstrated a crucial role of these fibres in executive aspects of language elaboration. Particularly, the functional analysis demonstrated the implication of the more medial component of this pathway in phonological network (Fig. 5a). These fibres describe a "C" course from the ventral cortices of the frontal lobe (particularly, IFG and MFG) to the temporal cortices (MFG, ITG, and STG), around the circular sulcus of the insula and outside from the EC (Fig. 5a–c). The functional response errors matched with the DTI reconstruction of the AF, as described by Catani et al. [Catani et al., 2002, 2005; Catani and ffytche, 2005; Catani and Mesulam, 2008; Thiebaut de Schotten et al., 2011]. Our results support the existence of anatomical background of a dorsal pathway dedicated to map verbal input onto articulatory-based representations, including the phonological elaboration [Axer et al., 2013; Hickok and Poeppel, 2004; Saur et al., 2008]. The distribution of the verbal apraxia deficits reported during the naming task further supports this hypothesis. These response errors show a similar distribution within the WM of the frontal lobe (particularly, the IFG, VPMC and MFG), but the course of the bundle subserving this function was mildly more lateral and runs up to the inferior cortices of the parietal lobe (particularly, SMG and AG), not reaching the temporal lobe (Fig. 5c). This distribution matches with the DTI course of the lateral indirect anterior component of the SLF, supporting the role of this portion as the articulatory loop of language production [Axer et al., 2013; Duffau, 2008]. Therefore, considering our results, the dorsal stream emerges as a parallel and dissociate network subserved by two different pathways: the medial one, corresponding to the AF, directly connecting the frontal and the temporal lobe, and the lateral one, corresponding to the indirect anterior portion of the SLF which connects the ventral and posterior cortices of the frontal lobe to the IPL [Makris et al., 2005].

The semantic paraphasias showed a different distribution within the WM connecting the temporo-parieto-occipital junction posteriorly, running along the horizontal associative fibers of the temporal lobe, over the roof of the temporal horn of the ventricle and in the most ventral portion of the EC, up to the frontal lobe (particularly, IFG, MFG, SFG) (Fig. 5b). This long ventral distribution of semantic errors, matches with the IFOF course as described by DTI reconstructions and anatomical dissections [Martino et al., 2009; Sarubbo et al., 2013; Thiebaut de Schotten et al., 2011; Thiebaut de Schotten et al., 2012]. These data support the previously hypothesized role of IFOF as the main stream of the semantic language network [Axer et al., 2013; Duffau, 2008; Moritz-Gasser et al., 2013; Sarubbo et al., 2013]. Interestingly, the functional response errors distributed along the vertical WM directed to the posterior and middle portions of the MFG (Fig. 5b) matches with the recent "post-mortem" dissection [Sarubbo et al., 2013] and "in vivo" DTI results [Lebel et al., 2012; Thiebaut de Schotten et al., 2012] which described a

new deeper and vertical portion of the IFOF directed to the dorsal cortices of the frontal lobe. A second "indirect" ventral pathway was proposed for semantic elaboration subserved by ILF and connecting the occipital and temporal inferior and basal cortices to the frontal lobe through the relay of the UF fibers, which run through the EC [Agosta et al., 2013; Saur et al., 2008]. In this series the UF resulted the most resected bundle for surgical reasons and our data do not support the role of this bundle in the semantic network, according to previous reports [Duffau et al., 2009]. Moreover, even if the overall distribution of the collected stimuli has a higher statistical and anatomical (particularly, the distribution of the response errors within the EC, frontal lobe and more medial WM of the temporal lobe) match with the course of the IFOF, we cannot rule out the role of the ILF in this dynamic, multimodal and pluri-component network [Duffau et al., 2013].

The reading deficits (i.e. alexia) were mostly reported along the associative WM running from the occipital lobe through the temporo-parieto-occipital junction to the temporo-basal and inferior cortices (Fig. 4c). These response errors matched with the course of the ILF. The literature lacks in conclusive functional data regarding the ILF. As previously discussed, the ILF was proposed as part of an "indirect" parallel ventral semantic stream, even if DES did not produce conclusive data supporting this hypothesis [Duffau et al., 2013; Mandonnet et al., 2007]. However, a possible role of this bundle in reading and visual-orthographic processing has been already hypothesized [Fernández-Miranda et al., 2008; Gil-Robles et al., 2013]. Our data support this hypothesis, especially regarding the most posterior portion of the bundle, demonstrating also a prominent involvement of the lateral occipital cortices and the temporal inferior and basal regions in visual elaboration of language input.

Pure anomia, not intended as motor, praxic or visual naming disturbances, but as lexical retrieval deficits, were reported at the junction between the inferior parietal lobule (SMG and AG, the so-called Geschwind's territories) and the posterior two-thirds of the STG and MTG (the so-called Wernicke's territories) (Fig. 5c). These data were expected, considering the hypothesized role of the cortices nearby the posterior third of the STS in lexical representation, including the STG and MTG [Lau et al., 2008]. Hickok and Poeppel (2007) proposed a hypothetical network, including the peri-STS as a crucial region for sensory coding of speech. The cortices around Sylvian fissure at the boundary between the parietal (i.e. SMG and AG) and temporal lobes (including the posterior peri-STS region) would be involved in sensory-motor integration of speech processing [Hickok et al., 2009]. The anomia registered in these regions are more lateral and posterior with respect to the speech arrest, verbal apraxia and phonological disorders, and extremely more dorsal and lateral in the WM of the temporo-parietal junction with respect to the semantic disorders (Figs. 3c; 5b,c). These functional response errors were elicitedin the more lateral long WM at the border between the IPL and the temporal lobe. By comparing the overall distribution of these stimuli with DTI, their locations match with the course of the indirect posterior portion of the SLF that connects the posterior cortices of the temporal lobe and peri-STC region to the AG and SMG of the IPL. This suggests a possible role of these fibers in the access and retrieval of semantic information for language elaboration. However, it is worth noting that the DTI Atlas we used [Thiebaut de Schotten et al., 2011] does not include the middle longitudinal fascicle (MdLF). This tract was first described by Makris et al. (2009) and it was proposed as a possible direct associative connection between these territories [Frey et al., 2008]. Therefore, we cannot rule out this anatomo-functional hypothesis. We demonstrated a wide distribution of the anomia in the lateral WM of the temporo-parieto-occipital junction. As recently described by our team [Chan-Seng et al., 2014; De Benedictis at al., 2014; Sarubbo et al., 2015], this region represents a crucial crossing area between several WM associative pathways including AF, SLF, IFOF, ILF, and MdLF. These bundles constitute the dorsal and the ventral direct and indirect streams deputed to different aspects of language processing. This highly integrated anatomo-functional organization led us to consider also a third hypothesis. In fact, even if we excluded responses associated with other language disturbances (i.e. semantic and phonological paraphasias, verbal apraxia, etc.), the anomia collected in this region could be also related to the contemporary deactivation of both the ventral and dorsal language pathways.

Our data confirm also the crucial role of the WM of the parietal lobe (particularly SMG up to the border with the STG and the region around the intraparietal sulcus in the right hemisphere) in spatial cognition. According to the DTI matching analysis, the response errors collected during the line bisection task were mostly located in the WM of the SLF and AF, lateral to the fibers of Cing and posterior to the vertical fibers of the CTT, as reported also in DTI and anatomical descriptions [De Benedictis et al., 2012; Sarubbo et al., 2013] as well as using DES [Thiebaut de Schotten et al., 2005].

Both the cortices of the fronto-medial and fronto-lateral regions, Cing and insula as well as the fibers terminating in these cortices were demonstrated to be crucial for awareness and control of voluntary movements [Brass and Haggard, 2008; Haggard, 2008; Hoffstaedter et al., 2013; Wolpe et al., 2014]. The anatomical background of this network is not yet completely identified because of the extreme complexity of the mutual connections including different frontal cortices (i.e. SMA, PreSMA, PreCS and DLPFC), Cing and insula, and also the deep nuclei [i.e. Caud, putamen, lenticular nucleus (Put and LN, respectively)]. However, these response errors could partly match with the course of the Frontal Aslant Tract. Our stimulation data demonstrated a prevalent distribution of the disorders in the voluntary movements organization (i.e. movement arrest, motor and verbal perseveration,

eyes apraxia) within the frontal lobe (particularly in the WM terminating in the SMA, PreSMA, SFG, and MedSFG and in contact to the WM of the anterior and middle portion of the cingulum) as well as in the deep nuclei, particularly in the Caud, pallidum and Put (Figs. 2a–c; 3b). Recent findings demonstrated a role of the fronto-medial cortices (particularly the pre-SMA) in movement selection and of the lateral frontal cortices (particularly the dorsal pre-motor cortex) in movement execution with a complex cortico-subcortical integration (including SMA, DLPFC, insula, basal ganglia) responsible for the timing of the voluntary movements execution [Hoffstaedter et al., 2013; Wolpe et al., 2014]. Here, DES of the WM terminating in the pre-SMA, SMA and the insula systematically elicited arrest of the motor task, confirming our previous study [Schucht et al., 2013], and confirming the functional organization previously proposed by demonstrating crucial hubs for the execution of voluntary movements within the medial cortices of the frontal lobe and the insula.

Limitations of the Study

The manual positioning of the functional sites recorded during surgery by mean of high-resolution pictures, constitute a possible limitation of this study. It is nonetheless worth noting that this method has already been used to elaborate both subcortical and cortical functional atlases [Ius et al., 2011; Tate et al., 2014] with a high level of reliability. Moreover, in order to improve the accuracy of the data, we adopted a multiplanar (axial, sagittal, and coronal) visualization of the postoperative MRI rotated according to the surgical position of each patient. Furthermore, all functional regions were accurately selected from the same operator, who is a neurosurgeon expert in brain surgery and WM anatomy. We also selected the 3-months postoperative MRIs and not the early postoperative MRIs. Indeed, the 3-months MRIs are more accurate because the limits of the surgical resection are well defined, oedema is resolved, the brain is completely re-expanded, and the coregistation procedure for the common MNI 152 space or templates is more precise. Moreover, the slow rate of the LGG's growth (4–5 mm of mean diameter/year) [Mandonnet et al., 2008] excluded gross morphological variation of eventual residuals.

Finally, we included in this functional atlas of the human WM fibers, data exclusively coming from a homogeneous group of patients affected by LGGs. Even if LGG can induce neuroplasticity, this phenomenon occurs mainly at the cortical level, with a very low plastic potential at the subcortical level [Ius et al., 2011]. Here, we report a probabilistic map focusing on the functional distribution of the WM pathways, thus with very low interferences of LGG with regard to the actual organization of the subcortical functions in normal brain. A limitation of this study regards the small sample sizes for some of the explored functions that, anyway, could be overpassed with future updates and with implementation of these probabilistic maps over the time. Moreover, the functional response errors collected and showed in our maps are strongly related to the limited series and features of neuropsychological test actually available for the intraoperative setting, as in the case of semantic deficits collected exclusively with a visual denomination task.

To sum up, "in vivo" DES in patients affected by LGGs were extensively adopted in the past for investigating brain processing, in particular the organization of large-distributed networks: it should be underlined these data were also shown to match with results provided by other techniques allowing the study of brain structure and function (i.e. DTI, fMRI, MEG, etc.), demonstrating the reliability of DES in awake patients [Duffau, 2012 and 2014; Ius et al., 2011; Tate et al., 2014].

CONCLUSIONS

For a long time, although the functional organization of the cortex was extensively studied, the subcortical connectivity has received less attention. Recent advances in DTI have allowed a better understanding of the WM anatomy, and resulted in the elaboration of an atlas dedicated to the fibers pathways [Catani and Thiebaut de Schotten, 2011]. However, no functional information has been provided. Here, we report the first anatomo-functional atlas of WM connectivity in humans, by correlating cognitive data issued from intraoperative subcortical electrostimulation mapping and surgical cavities superimposed on anatomical DTI atlas in a large population. Our subcortical atlas of brain functions could have major implications both in the field of cognitive neurosciences as well as in clinical practice, especially for brain surgery.

REFERENCES

Agosta F, Galantucci S, Canu E, Cappa SF, Magnani G, Franceschi M, Falini A, Comi G, Filippi M (2013): Disruption of structural connectivity along the dorsal and ventral language pathways in patients with nonfluent and semantic variant primary progressive aphasia: A DT MRI study and a literature review. Brain Lang 127:157–166.

Axer H, Klingner CM, Prescher A (2013): Fiber anatomy of dorsal and ventral language streams. Brain Lang 127:192–204.

Bartolomeo P, Thiebaut de Schotten M, Duffau H (2007): Mapping of visuospatial functions during brain surgery: A new tool to prevent unilateral spatial neglect. Neurosurgery 61:E1340

Berger MS, Ojemann GA, Lettich E (1990): Neurophysiological monitoring during astrocytoma surgery. Neurosurg Clin N Am 1:65–80.

Borner K, Sanyal S, Vespignani A (2007): Network science. Annu Rev Inform Sci Tech 41:537–607.

Brass M, Haggard P (2008): The what, when, whether model of intentional action. Neuroscientist 14:319–325.

Bressler SL, Tognoli E (2006): Operational principles of neurocognitive networks. Int J Psychophysiol 60:139–148.

Catani M, ffytche DH (2005): The rises and falls of disconnection syndromes. Brain 128:2224–2239.

Catani M, Howard RJ, Pajevic S, Jones DK (2002): Virtual in vivo interactive dissection of white matter fasciculi in the human brain. Neuroimage 17:77–94.

Catani M, Mesulam M (2008): The arcuate fasciculus and the disconnection theme in language and aphasia: History and current state. Cortex 44:953–961.

Catani M, Jones DK, ffytche DH (2005): Perisylvian language networks of the human brain. Ann Neurol 57:8–16.

Catani M, Thiebaut de Schotten (2013): Atlas of Human Brain Connections, Oxford University Press, USA

Chan-Seng E, Moritz-Gasser S, Duffau H (2014): Awake mapping for low-grade gliomas involving the left sagittal stratum: Anatomofunctional and surgical considerations. J Neurosurg 120: 1069–1077.

Collin G, Sporns O, Mandl RC, van den Heuvel MP (2014): Structural and functional aspects relating to cost and benefit of rich club organization in the human cerebral cortex. Cereb Cortex 29:2258–2267.

De Benedictis A, Sarubbo S, Duffau H (2012): Subcortical surgical anatomy of the lateral frontal region: Human white matter dissection and correlations with functional insights provided by intraoperative direct brain stimulation: Laboratory investigation. J Neurosurg 117:1053–1069.

De Benedictis A, Duffau H, Paradiso B, Grandi E, Balbi S, Granieri E, Colarusso E, Chioffi F, Marras CE, Sarubbo S (2014): Anatomo-functional study of the temporo-parieto-occipital region: dissection, tractographic and brain mapping evidence from a neurosurgical perspective. J Anat 225:132–151.

Duffau H (2005): Lessons from brain mapping in surgery for low-grade glioma: Insights into associations between tumour and brain plasticity. Lancet Neurol 4:476–486.

Duffau H (2008): The anatomo-functional connectivity of language revisited: New insights provided by electrostimulation and tractography. Neuropsychologia 46:927–934.

Duffau H (2009): A personal consecutive series of surgically treated 51 cases of insular WHO Grade II glioma: Advances and limitations. J Neurosurg 110:696–708.

Duffau H (2012): The "frontal syndrome" revisited: Lessons from electrostimulation mapping studies.Cortex 48:120–131.

Duffau H (2014): The huge plastic potential of adult brain and the role of connectomics: New insights provided by serial mappings in glioma surgery. Cortex 58:325–337.

Duffau H, Capelle L, Denvil D, Sichez N, Gatignol P, Lopes M, Mitchell MC, Sichez JP, Van Effenterre R (2003a): Functional recovery after surgical resection of low grade gliomas in eloquent brain: hypothesis of brain compensation. J Neurol Neurosurg Psychiatry 74:901–907.

Duffau H, Gatignol P, Denvil D, Lopes M, Capelle L (2003b): The articulatory loop: Study of the subcortical connectivity by electrostimulation. Neuro report 14:2005–2008.

Duffau H, Gatignol P, Mandonnet E, Peruzzi P, Tzourio-Mazoyer N, Capelle L (2005): New insights into the anatomo-functional connectivity of the semantic system: A study using cortico-subcortical electrostimulations. Brain 128:797–810.

Duffau H, Gatignol P, Moritz-Gasser S, Mandonnet E (2009): Is the left uncinate fasciculus essential for language? A cerebral stimulation study. J Neurol 256:382–389.

Duffau H, Herbet G, Moritz-Gasser S (2013): Toward a pluricomponent, multimodal, and dynamic organization of the ventral semantic stream in humans: Lessons from stimulation mapping in awake patients. Front Syst Neurosci 7:44.

Evans AC, Marrett S, Neelin P, Collins L, Worsley K, Dai W, Milot S, Meyer E, Bub D (1992): Anatomical mapping of functional activation in stereotactic coordinate space. Neuroimage 1:43–53.

Fernández-Miranda JC, Rhoton AL, Alvarez-Linera J, Kakizawa Y, Choi C, de Oliveira EP (2008): Three-dimensional micro- surgical and tractographic anatomy of the white matter of the human brain. Neurosurgery 62:989–1026.

Fernández Coello A, Moritz-Gasser S, Martino J, Martinoni M, Matsuda R, Duffau H (2013): Selection of intraoperative tasks for awake mapping based on relationships between tumor location and functional networks. J Neurosurg 119:1380–1394.

Filley CM (2005): White matter and behavioral neurology. Ann NY Acad Sci 1064:162–183.

Frey S, Campbell JS, Pike GB, Petrides M (2008): Dissociating the human language pathways with high angular resolution diffusion fiber tractography. J Neurosci 28:11435–11444.

Gil-Robles S, Carvallo A, Jimenez Mdel M, Gomez Caicoya A, Martinez R, Ruiz-Ocaña C, Duffau H (2013): Double dissociation between visual recognition and picture naming: A study of the visual language connectivity using tractography and brain stimulation. Neurosurgery 72:678–686.

Goodglass H, Kaplan E (1972): The Assessment of Aphasia and Related Disorders. Philadelphia, Pa: Lea and Fibiger.

Gras-Combe G, Moritz-Gasser S, Herbet G, Duffau H (2012): Intraoperative subcortical electrical mapping of optic radiations in awake surgery for glioma involving visual pathways. J Neurosurg 117:466–473.

Haggard P (2008): Human volition: Towards a neuroscience of will. Nat Rev Neurosci 9:934–946.

Hickok G, Poeppel D (2004): Dorsal and ventral streams: A framework for understanding aspects of the functional anatomy of language. Cognition 92:67–99.

Hickok G, Poeppel D (2007): The cortical organization of speech processing. Nat Rev Neurosci 8:393–402.

Hickok G, Okada K, Serences JT (2009): Area Spt in the human planum temporale supports sensory-motor integration for speech processing. J Neurophysiol 101:2725–2732.

Hoffstaedter F, Grefkes C, Zilles K, Eickhoff SB (2013): The "what" and "when" of self-initiated movements. Cereb Cortex 23:520–530.

Ius T, Angelini E, Thiebaut de Schotten M, Mandonnet E, Duffau H (2011): Evidence for potentials and limitations of brain plasticity using an atlas of functional resectability of WHO grade II gliomas: Towards a "minimal common brain". Neuroimage 56: 992–1000.

Krainik A, Duffau H, Capelle L, Cornu P, Boch AL, Mangin JF, Le Bihan D, Marsault C, Chiras J, Lehéricy S (2004): Role of the healthy hemisphere in recovery after resection of the supplementary motor area. Neurology 62:1323–1332.

Lau EF, Phillips C, Poeppel D (2008): A cortical network for semantics: (de)constructing the N400. Nat Rev Neurosci 9:920–933.

Lebel C, Gee M, Camicioli R, Wieler M, Martin W, Beaulieu C (2012): Diffusion tensor imaging of white matter tract evolution over the lifespan. Neuroimage 60:340–352.

Makris N, Kennedy DN, McInerney S, Sorensen AG, Wang R, Caviness VS Jr, Pandya DN (2005): Segmentation of subcomponents within the superior longitudinal fascicle in humans: A quantitative, in vivo, DT-MRI study. Cereb Cortex 15:854–869.

Makris N, Papadimitriou GM, Kaiser JR, Sorg S, Kennedy DN, Pandya DN (2009): Delineation of the middle longitudinal fascicle in humans: A quantitative, in vivo, DT-MRI study. Cereb Cortex 19:777–785.

Mandonnet E, Nouet A, Gatignol P, Capelle L, Duffau H (2007): Does the left inferior longitudinal fasciculus play a role in language? A brain stimulation study. Brain 130:623–629.

Mandonnet E, Pallud J, Clatz O, Taillandier L, Konukoglu E, Duffau H, Capelle L (2008): Computational modeling of the WHO grade II glioma dynamics: Principles and applications to management paradigm. Neurosurg Rev 31:263–269.

Martino J, Brogna C, Robles SG, Vergani F, Duffau H (2009): Anatomic dissection of the inferior fronto-occipital fasciculus revisited in the lights of brain stimulation data. Cortex 46:691–699.

McIntosh AR (2000): Towards a network theory of cognition. Neural Netw 13:861–870.

Metz-Lutz M, Kremin H, Deloche G, Hannequin D, Ferrand L, Perrier D (1991): Standardisation d'un test de dénomination orale: controle des effets de l'age, du sexe et du niveau de scolarité chez les sujets adultes normaux. Rev Neuropsychol 1: 73–95.

Moritz-Gasser S, Herbet G, Duffau H (2013): Mapping the connectivity underlying multimodal (verbal and non-verbal) semantic processing: A brain electrostimulation study. Neuropsychologia 51:1814–1822.

Ojemann G, Ojemann J, Lettich E, Berger M (1989): Cortical language localization in left, dominant hemisphere. An electrical stimulation mapping investigation in 117 patients. J Neurosurg 71:316–326.

Reijneveld JC, Ponten SC, Berendse HW, Stam CJ (2007): The application of graph theoretical analysis to complex networks in the brain. Clin Neurophysiol 118:2317–2331.

Sarubbo S, Latini F, Sette E, Milani P, Granieri E, Fainardi E, Cavallo MA (2012a): Is the resection of gliomas in Wernicke's area reliable? Wernicke's area resection. Acta Neurochir (Wien) 154:1653–1662.

Sarubbo S, Le Bars E, Moritz-Gasser S, Duffau H (2012b): Complete recovery after surgical resection of left Wernicke's area in awake patient: A brain stimulation and functional MRI study. Neurosurg Rev 35:287–292.

Sarubbo S, De Benedictis A, Maldonado IL, Basso G, Duffau H (2013): Frontal terminations for the inferior fronto-occipital fascicle: Anatomical dissection, DTI study and functional considerations on a multi-component bundle. Brain Struct Funct 218: 21–37.

Sarubbo S, De Benedictis A, Milani P, Paradiso B, Barbareschi M, Rozzanigo U, Colarusso E, Tugnoli V, Farneti M, Granieri E, Duffau H, Chioffi F (2015): The course and the anatomofunctional relationships of the optic radiation: A combined study with "post mortem" dissections and "in vivo" direct electrical mapping. J Anat 226:47–59.

Saur D, Kreher BW, Schnell S, Kümmerer D, Kellmeyer P, Vry MS, Umarova R, Musso M, Glauche V, Abel S, Huber W, Rijntjes M, Hennig J, Weiller C (2008): Ventral and dorsal pathways for language. Proc Natl Acad Sci USA 105:18035–18040.

Schucht P, Moritz-Gasser S, Herbet G, Raabe A, Duffau H (2013): Subcortical electrostimulation to identify network subserving motor control. Hum Brain Mapp 34:3023–3030.

Sporns O (2013a): Structure and function of complex brain networks. Dialogues Clin Neurosci 15:247–262.

Sporns O (2013b): The human connectome: Origins and challenges. Neuroimage 80:53–61.

Sporns O, Tononi G, Kötter R (2005): The human connectome: A structural description of the human brain. PLoS Comput Biol 1:e42.

Tate MC, Herbet G, Moritz-Gasser S, Tate JE, Duffau H (2014): Probabilistic map of critical functional regions of the human cerebral cortex: Broca's area revisited. Brain 137:2773–2782.

Thiebaut de Schotten M, Urbanski M, Duffau H, Volle E, Lévy R, Dubois B, Bartolomeo P (2005): Direct evidence for a parietal-frontal pathway subserving spatial awareness in humans. Science 309:2226–2228.

Thiebaut de Schotten M, Ffytche DH, Bizzi A, Dell'Acqua F, Allin M, Walshe M, Murray R, Williams SC, Murphy DG, Catani M (2011): Atlasing location, asymmetry and inter-subject variability of white matter tracts in the human brain with MR diffusion tractography. Neuroimage 54:49–59.

Thiebaut de Schotten M, Dell'Acqua F, Valabregue R, Catani M (2012): Monkey to human comparative anatomy of the frontal lobe association tracts. Cortex 48:82–96.

Tzourio-Mazoyer N, Landeau B, Papathanassiou D, Crivello F, Etard O, Delcroix N, Mazoyer B, Joliot M (2002): Automated anatomical labeling of activations in SPM using a macroscopic anatomical parcellation of the MNI MRI single-subject brain. Neuroimage 15:273–289.

Wolpe N, Moore JW, Rae CL, Rittman T, Altena E, Haggard P, Rowe JB (2014): The medial frontal-prefrontal network for altered awareness and control of action in corticobasal syndrome. Brain 137:208–220.